Solid State Ionics 180 (2010) 1652–1659

Contents lists available at ScienceDirect

Solid State Ionics

journal homepage: www.elsevier.com/locate/ssi

Structure of Li_2MnO_3 with different degrees of defects

A. Boulineau [a,b], L. Croguennec [a,b], C. Delmas [a,b], F. Weill [a,b,c,*]

[a] CNRS, ICMCB, 87 avenue du Dr. A. Schweitzer, PESSAC, F-33608, France
[b] Université de Bordeaux, ICMCB, ENSCPB, PESSAC, F-33608, France
[c] Université de Bordeaux, CREMEM, TALENCE, F-33405, France

ARTICLE INFO

Article history:
Received 30 March 2009
Received in revised form 14 September 2009
Accepted 28 October 2009

Keywords:
Li_2MnO_3
Layered oxides
X-ray diffraction
Electron diffraction
Defects
Stacking faults

ABSTRACT

The synthesis and structural properties of the layered oxide Li_2MnO_3 have been studied in details. It represents a key for a better understanding of the complex structural evolutions pointed out in the materials like Li(Li,Ni,Mn,Co)O_2 when they are used as positive electrode materials in lithium-ion batteries. Li_2MnO_3 samples were prepared either via coprecipitation or via a two step solid state reaction followed by different annealing treatments. Using X-ray and electron diffraction in combination with diffraction data simulations, we show that in function of the synthesis conditions, Li_2MnO_3 is obtained with various degrees of disorder, along the *c* monoclinic direction, in the stacking of the ordered $Li_{1/3}Mn_{2/3}$ sheets within the cfc oxygen packing. We show that this disorder decreases when the synthesis temperature increases but the synthesis of a material free of stacking faults is not possible with these synthesis routes. Finally, the similarities between the evolutions pointed out in Li_2MnO_3 due to the synthesis conditions and those previously observed in the materials like Li(Li,Ni,Mn,Co)O_2 related to the evolution of the cations distribution in the slabs are underlined.

1. Introduction

The main material used as positive electrode in lithium-ion batteries remains the $LiCoO_2$ layered oxide. But, despite good electrochemical performances [1], the limited availability of cobalt makes this material expensive and limits thus its use to small cells. $LiNiO_2$ derivatives, such as $LiNi_{1-x-y}Co_xAl_yO_2$, were found to be a good alternative for large scale applications as they deliver high energy and power densities [2]. For transport applications, such as for hybrid and electric vehicles, safety remains the main concern for most of the materials: indeed they can be highly unstable in the very delithiated state (overcharged state of the battery) with possible loss of oxygen and heat generation through reaction of this oxygen with the liquid organic electrolyte [3]. More recently, the layered transition metal oxides $Li_{1+x}(Ni_{1/2-y}Mn_{1/2-y}Co_{2y})_{1-x}O_2$ have attracted much attention due to their large capacity and good cyclability, with a much higher thermal stability in the desintercalated state (increase of the decomposition temperature from 70 °C to 100 °C *vs.* $LiNi_{1-x-y}Co_xAl_yO_2$) [4–9]. These systems contain of Ni^{2+}, Ni^{3+}, Mn^{4+} and Co^{3+} ions, the Mn^{4+} ions being at the origin of their largely improved chemical and thermal stability. From a structural point of view, these Mn^{4+}-rich compounds appear complex. They can still be described as O3-type structures, but with lithium ions sitting both in the slab and in the interslab space and with the formation a cation ordering in the transition metal layers. This cation ordering in the slabs (superstructures in the *(a, b)* planes) is very similar to that reported for Li_2MnO_3, nevertheless the existence of diffusion in the X-ray and electron diffraction patterns [10] makes difficult to explain what is going on in the third dimension (along the *c*-axis). Li_2MnO_3 being viewed as a model compound for this system, because of its structural similarities, we decided to revisit its chemistry and structural properties.

The chemical formula Li_2MnO_3 can be written as $Li[Li_{1/3}Mn_{2/3}]O_2$ and can thus be described as $LiMO_2$ layered compounds; it is an O3-type structure where interslab octahedral sites are only occupied by lithium ions whereas slab octahedral sites are occupied by lithium and manganese ions in proportion (1:2). Due to the differences in ionic radii between Li^+ and Mn^{4+} (0.74 and 0.54 Å respectively [12]), these ions are ordered in the slabs to minimize the strains. The stacking along *c* of these ordered cationic planes is responsible for the reduction of the symmetry from the trigonal symmetry of the O3-type structure (R-3m) to the monoclinic one of Li_2MnO_3 (C2/*m*) This structure has been determined by Strobel et al. [11] using single crystal X-ray diffraction. The unit cell parameters are $a_{mon}=4.937(1)$ Å, $b_{mon.}=8.532(1)$ Å, $c_{mon.}=5.030(2)$ Å and $\beta=109.46(3)°$. Lithium ions occupy the 2b (0, 1/2, 0), 2c (0, 0, ½) and 4 h (0, 0.66, ½) sites, the manganese ions, the 4 g (0, 0.167, 0) site, and the oxygen ions, the 4i (0.219, 0, 0.227) and 8j (0.254, 0.321, 0.223) sites.

However, due to difficulties in modeling the experimental X-ray diffraction pattern profile and because of uncertainty in the interpretation of electron diffraction patterns, discrepancies still exist in the literature about the stacking sequence of the ordered

* Corresponding author. CNRS, ICMCB, 87 avenue du Dr. A. Schweitzer, PESSAC, F-33608, France. Tel.: +33 5 40 00 26 54; fax: +33 5 40 00 27 61.
E-mail address: weill@icmcb-bordeaux.cnrs.fr (F. Weill).

0167-2738/$ – see front matter © 2009 Elsevier B.V. All rights reserved.
doi:10.1016/j.ssi.2009.10.020

transition metal layers in Li_2MnO_3 [13–19]. Here, we report on the influence of the synthesis on the structure of Li_2MnO_3, not with the aim to compare two synthesis methods but to prepare different Li_2MnO_3 samples showing various degrees of defects. The characterization of these defects should help to get a clearer view of the changes occurring in materials like $Li(Li,Ni,Mn,Co)O_2$ depending on the composition. For that purpose, we will also compare the results obtained in the present study with some already published by some of us concerning the $Li_{1+x}(Ni_{1/2-y}Mn_{1/2-y}Co_{2y})_{1-x}O_2$ materials [9]. Note also that a detailed HRTEM and electron diffraction study of one of the Li_2MnO_3 sample presented here is reported elsewhere [20].

2. Experimental

2.1. Synthesis

Li_2MnO_3 samples were prepared by two synthesis routes: one based on a coprecipitation method, and the other on a two step solid state method, to get Li_2MnO_3 samples with different structural properties.

The coprecipitation route consisted of dripping slowly an aqueous solution of $Mn(NO_3)_2$ (Fluka 98%) into a stirred solution of LiOH (Alfa Aesar 98%), whose volume was adjusted to ensure a stoichiometric ratio (Li/Mn = 2). The as obtained precipitate was dried at 80 °C in a rotavapor, ground and then heated in air at 650 °C during 12 h to ensure the decomposition of the nitrates and the formation of the lithiated layered oxides. Two samples were finally obtained after a second annealing in air, either at 650 °C or at 850 °C for 24 h.

The two step solid state synthesis was performed according to [21]. The first step consists in the addition of 5 g of $KMnO_4$ (Prolabo 99%) in 400 ml of distilled water with 5 ml of ethanol. The mixture is maintained in a stainless steel autoclave at 100 °C during 24 h under stirring. This step leads to the formation of a nanosized MnO(OH) powder. The prepared highly divided material was washed with distilled water and then acetone, and dried at 80 °C during about 60 h. MnO(OH) was then ground with an excess of LiOH (molar ratio Li/Mn = 2.1) to ensure the stoichiometry in spite of lithium vaporisation during the annealing treatment. Finally, the powder was washed again with distilled water and then with acetone to remove the excess of lithium source that wouldn't have reacted, and then dried at 80 °C. Two samples were finally obtained after an annealing in air, either at 800 °C or at 900 °C for 4 h.

2.2. Chemical, redox and thermogravimetric analyses

The Li/Mn ratio was determined using an inductively coupled plasma optical emission spectrometer (ICP-OES), (Varian 720-ES) after the complete dissolution of the powder into an acidic solution. The uncertainty of the measurement is about 0.03 Li per atomic formula.

The average oxidation state of manganese in the various materials was determined by iodometric back titration: the sample was dissolved at 60 °C overnight in an aqueous solution of HCl and KI, and then the resulting solution was titrated with $Na_2S_2O_3$. Note that the whole process including sample dissolution was performed at least twice.

The thermogravimetric analysis (TGA) was performed using a STD Q600 Texas Instrument apparatus. Measurements were carried out from room temperature to 900 °C at a constant heating rate of 5 °C/min, under a flow of oxygen and with about 40 mg of Li_2MnO_3 powder. Alumina sample holder was also used as reference sample.

2.3. X-ray diffraction characterization

The X-ray diffraction (XRD) patterns of the four samples were collected at room temperature using the Cu Kα radiation on a Siemens D5000 diffractometer in the θ–θ Bragg–Brentano geometry. The patterns were recorded in the 2θ range 10–120°, making 2θ step-scan intervals of 0.02° with a constant counting time of 45 s. The patterns were analyzed by the Rietveld method as implemented in the program Fullprof [22]. Powder X-ray diffraction simulations were performed with the DIFFAX software, developed by Treacy and Newsam [23], in order to quantify the amount of stacking faults in these materials.

2.4. Electron diffraction investigation

Electron diffraction patterns were collected with a JEOL 2000FX microscope equipped with a double tilt specimen holder. It was used at an accelerating voltage of 200 kV. The grids observed were prepared by dropping them in a suspension of ground material dispersed in ethanol. Selected Area Electron Diffraction patterns were simulated along the [110] monoclinic zone axis using the DIFFAX software in order to illustrate the influence in the electron diffraction pattern of faults in the slabs stacking. Our present study highlights the previous observation we made on the $Li_{1+x}(Ni_{1/2-y}Mn_{1/2-y}Co_{2y})_{1-x}O_2$ materials. All information about the synthesis and the characterisation of these materials can be found in reference [9].

3. Results and discussion

3.1. Thermogravimetric analyses

As shown in Fig. 1, a TGA analysis of a LiOH and γ-MnOOH mixture (such as Li/Mn atomic ratio = 2.3) was performed in order to follow the formation of Li_2MnO_3. Desorption of adsorbed water on γ-MnOOH is at the origin of the first weight loss (~7%wt.) observed until ~80 °C, the first step of this thermal analysis reveals thus that the true nominal LiOH/γ-MnOOH molar ratio is closer to 2.49 than to 2.3. The loss of mass occurring above 80 °C (~14%wt.) is in good agreement with the formation of Li_2MnO_3 from a mixture of LiOH and γ-MnOOH. The plateau observed above 550 °C shows that Li_2MnO_3 is stable until ~800 °C. The further loss of weight above 800 °C is associated at least to oxygen loss as it will be described in detail elsewhere [24]. This thermogravimetric analysis reveals thus that Li_2MnO_3 can be obtained from a mixture of LiOH and γ-MnOOH heated above 550 °C. The four samples synthesised here are for two of them in the thermal stability domain of Li_2MnO_3, whereas the two others are at its frontier.

3.2. XRD patterns refinement and their simulations

The X-ray diffraction patterns of the Li_2MnO_3 samples are given in Fig. 2. All the reflections can be indexed in the monoclinic system

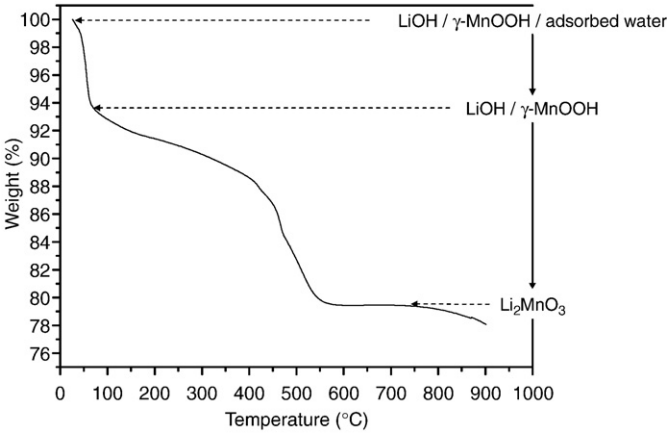

Fig. 1. Thermogravimetric analysis performed for a mixture of LiOH and γ-MnOOH in the molar ratio 2.3:1, at a constant heating rate of 5 °C/min, under a flow of oxygen.

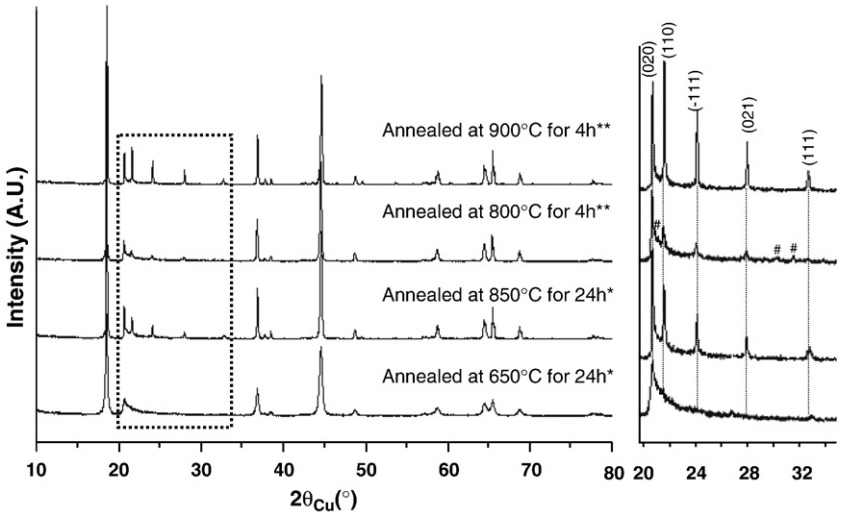

Fig. 2. Comparison of the XRD patterns collected for Li_2MnO_3 compounds obtained by two different synthesis routes: *coprecipitation and **solid state synthesis. The enlargement of the 19.5–35° $2\theta_{Cu}$ angular range is also given. #: Li_2CO_3 impurity.

using the space group *C2/m*. When the synthesis is performed at high temperature (900 °C) all the peaks are really sharp, indicating the formation of a well crystallized material. A broadening is observed when the synthesis temperature decreases, especially huge for the reflections related to the Li/Mn ordering in the slabs, *i.e.* reflections (020), (110), (-111), (021) and (111) in the 20–34° $2\theta_{Cu}$ range. Note that for the coprecipitated powder annealed at 650 °C the broadening is so huge that the reflections (020), (110), (−111) and (021) are convoluted in a unique asymmetric diffuse peak.

The four samples present average manganese oxidation state and Li/Mn ratio close to 4 and 2 respectively, leading for the first three samples to a global chemical formula very close to that expected, see Table 1. In good agreement with the TGA results discussed just before, the sample obtained through the solid state reaction at 900 °C was found to be obviously deficient in oxygen. This discrepancy with the ideal stoichiometry has been studied in detail and was shown to be due to the presence of spinel-type defects at the surface of the particles [24]. Note nevertheless that the small deviation from the ideal stoichiometry expected for samples annealed at 800 °C and 850 °C from the TGA experiments has not been detected by chemical analyses (probably because it is within the limit of the technique).

These four XRD patterns were refined according to the procedure detailed hereafter for the compound obtained through the solid state synthesis route and annealed at 900 °C. We chose to begin the XRD refinement by this material since it presents the better defined reflections. In the X-ray refinement of this material, we considered the bulk stoichiometry to be Li_2MnO_3 and we neglected the spinel-type defect responsible for the deviation of the global stoichiometry from the ideal one. Due to the presence of diffusion especially in the 20–26° (2θ) range, the background was modeled with great care using an interpolated background, then the structural and profile parameters (according to a pseudo-Voigt profile function for these latter) were refined using the following order: *(i)* scale factor and sample displacement correction, *(ii)* cell parameters, *(iii)* profile parameters, *(iv)* atomic positions, *(v)* sites occupancies and *(vi)* isotropic atomic thermal displacement parameters (B_{iso}). 19 parameters were finally refined (on the basis of 171 reflections). The first refinement was carried out considering the ideal cation distribution, so in accordance with the formula $\{(Li_2)_{2c}(Li_4)_{4\ h}\}_{interslab}\{(Li_2)_{2b}(Mn_4)_{4\ g}\}_{slab}(O_{12})_{4i,8j}$. Refined lithium thermal displacement parameters on the 2c, 4 h and 2b sites were found equal to 2.2(9) Å², −3.7(5) Å² and −5.2(2) Å² respectively, that of manganese on the 4 g site was found equal to 0.55(5) Å² and those of oxygen on the 4i and 8j sites were found equal to 0.2(2) Å² and 0.2(1) Å² respectively ; the as obtained conventional Rietveld *R*-factors for points with Bragg contribution were $R_{wp} = 29.7\%$ and $R_{Bragg} = 11.5\%$ with $S_{cor} = 3.02$. The large negative values obtained for the thermal displacement parameters on the 4 h and 2b lithium sites suggested an electronic density excess that led us to consider a possible Li/Mn exchange between the 4 h and 4 g sites on one side and between the 2b and 4 g sites on the other side in accordance with the formula $\{(Li_2)_{2c}(Li_{4-y}Mn_y)_{4\ h}\}_{interslab}\{(Li_{2-z}Mn_z)_{2b}(Mn_{4-y-z}Li_{y+z})_{4\ g}\}_{slab}(O_{12})_{4i,8j}$. The 4 cation crystallographic sites were still considered to be fully occupied. As the simultaneous refinement of the site occupancies and the thermal displacement parameters led to the divergence of the latter, the lithium sites B_{iso} were thus fixed to 1.0 Å², the manganese site B_{iso} to 0.5 Å² and the oxygen site B_{iso} to 0.8 Å², in good agreement with those already reported for other $LiMO_2$ materials [25]. The comparison of the experimental and calculated X-ray diffraction patterns for this sample is presented in Fig. 3, and the structural and profile parameters obtained are reported in Table 2. In spite of a rather good minimization of the difference between the observed and the calculated intensities, the fit to the profile and the reliability factors remain rather poor. This is due to differential line broadenings of the reflexions, and especially to the broadening of the bottom of the (020) and (110) peaks as shown in insert in Fig. 3. The as refined unit cell parameters are close to those reported by Strobel et al. on single crystal [11]. The exchange ratio between the Mn ions from the slab (4 g site) and the Li ions from the interslab space (4 h site) is very small, only 0.06 ions are exchanged, whereas around 0.29 ions are exchanged between the Mn 4 g and Li 2b sites in the slabs leading to the crystallographic formula $\{(Li_2)_{2c}(Li_{3.94}Mn_{0.06})_{4h}\}_{interslab}\{(Li_{1.71}Mn_{0.29})_{2b}(Mn_{3.65}Li_{0.35})_{4g}\}_{slab}(O_{12})_{4i,8j}$.

Table 3 sums up the cell and structural parameters obtained for the fours powders via the Rietveld refinement of their XRD data. The sites occupancies present some significant changes depending on the synthesis conditions. The lower the temperature of the annealing treatment the higher is the percentage of manganese ions in the

Table 1
Manganese average oxidation states, Li/Mn ratios and global chemical composition deduced from these chemical and redox analyses for the Li_2MnO_3 samples obtained in different synthesis conditions.

Synthesis route	Annealing treatment	Mn average oxidation state[a]	Li/Mn ratio[a]	Chemical composition
Coprecipitation	650 °C for 24 h	4.02	2.01	$Li_{2.01}MnO_{3.01}$
	850 °C for 24 h	4.05	2.04	$Li_{2.04}MnO_{3.04}$
Solid state	800 °C for 4 h	4.10	1.97	$Li_{1.97}MnO_{3.03}$
	900 °C for 4 h	3.85	1.96	$Li_{1.96}MnO_{2.91}$

[a] Obtained by chemical titration.

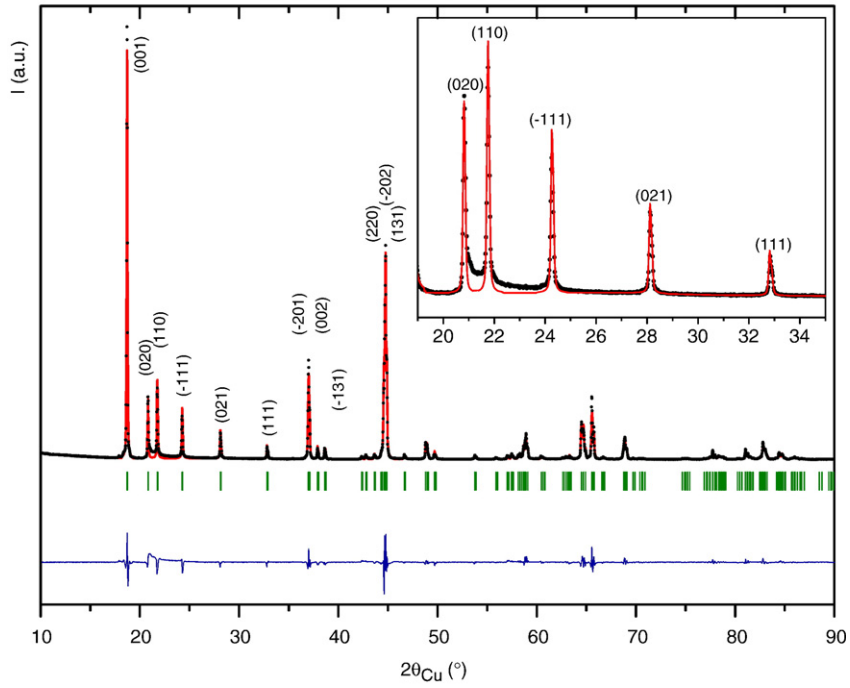

Fig. 3. Rietveld plot of the Li_2MnO_3 powder synthesised at 900 °C for 4 h by the solid state reaction. Detail of the reflections related to the Li/Mn ordering in the slabs is given in insert. The 90–120° (2θ) range is not presented to enlarge the figure.

interslabs (y/6) and the higher is the percentage of manganese ions in the lithium sites from the slabs (z/2). An increase in the annealing temperature tends thus to lead to a material closer and closer to the ideal one, *i.e.* with a cation distribution in agreement with $\{(Li_2)_{2c}(Li_4)_{4h}\}_{interslab}\{(Li_2)_{2b}(Mn_4)_{4g}\}_{slab}(O_{12})_{4i,8j}$. Note nevertheless that whatever the synthesis conditions chosen in this study the Li/Mn exchange in the slabs remain significant (~15 at.%).

In a perfect Li_2MnO_3 compound, all the ordered $(Li_{1/3}Mn_{2/3})$ cationic planes are stacked along the $c_{mon.}$ axis according to a unique stacking vector which is the $\overrightarrow{C_{mon}}$ translation. Note that the refinements described just before were performed according to such an hypothesis. Nevertheless as proposed at first by Lang [13], and more recently by Bréger et al. [14], two other stacking vectors exist and would lead to stacking very close in energy (1 or 2 meV of difference); their statistical occurrence would generate so called "stacking faults". To quantify the effect of such stacking faults on the X-ray diffraction pattern of Li_2MnO_3, we performed simulations by the means of the DIFFAX software. Such simulations require to define primary blocks which are then stacked. To describe Li_2MnO_3 a unique type of blocks constituted by a slab and an interslab space has been considered, each block being stacked over the previous one according to one of the three possible stacking vectors, whose coordinates are (0; 0; 1) (1/2; −1/6; 1) and (1/6; −1/6; 1) in the monoclinic system. Note that all the simulations were done in the hypothesis of an LiO_2 interslab between each $(Li_{1/3}Mn_{2/3})O_2$ slab. The exclusive occurrence of one of this vector leads to the perfect stacking but their alternations create stacking faults. Probabilities are affected to the three vectors so that the quantity of stacking faults occurring statistically is well known and imposed. As shown in Fig. 4, probabilities of faults have been varied continuously from 0 to 100%. Note that the increasing amount of stacking faults induces a continuous broadening of the (020), (110), (−111), (021) and (111) diffraction lines in the 20–34° $2\theta_{Cu}$ range, in good agreement with the decreasing coherent domain size of the ordered domains. Furthermore, by comparing the intensities ratio of the experimental (110) and (020) peaks ($I_{(110)}/I_{(020)}$) with the calculated ones, we could roughly estimate the percentage of stacking faults in each Li_2MnO_3 sample we prepared. Calculated X-ray diffraction patterns with a given amount of stacking faults and corresponding rather well to the experimental patterns are given for an easier comparison in Fig. 5. According to those simulations, a higher annealing temperature implies a decrease in the amount of stacking faults.

Nevertheless, as shown in Fig. 6a for Li_2MnO_3 obtained by solid state reaction at 800 °C, the experimental (020), (110), (−111), (021) and (111) diffraction lines remain sharper than expected considering 20% of statistically distributed stacking faults: this reveals that the coherence domain length of the ideally ordered domains remains larger than expected and thus that there is a concentration of stacking faults in given zones of the crystals (*i.e.* a deviation from the statistic).

Table 2
Structural and profile parameters obtained from the refinement by the Rietveld method of the X-Ray diffraction data recorded for Li_2MnO_3 synthesised at 900 °C for 4 h by the solid state route.

Li_2MnO_3 synthesised at 900 °C for 4 h by the solid state reaction						
Space group: *C2/m*		Constraints:				
$a = 4.9292(2)$ Å		• Full occupancy of each crystallographic position				
$b = 8.5315(2)$ Å		• Li/Mn exchange between the *4g* and (*2b*, *4h*) sites				
$c = 5.0251(1)$ Å		• Stoichiometry constrained to Li_2MnO_3				
$\beta = 109.337(2)°$						
Atom	Site	Wyckoff positions			Occupancy	B_{iso} (Å²)
Li (1)	2b	0	1/2	0	0.854(4)	1
Mn (1)	2b	0	1/2	0	0.146(4)	1
Li (2)	2c	0	0	1/2	1	1
Li (3)	4 h	0	0.681(2)	1/2	0.986(3)	1
Mn (2)	4 h	0	0.681(2)	1/2	0.014(3)	1
Li (4)	4 g	0	0.1687(3)	0	0.087(5)	0.5
Mn (3)	4 g	0	0.1687(3)	0	0.913(5)	0.5
O (1)	4i	0.224(2)	0	0.225(1)	1	0.8
O (2)	8j	0.253(1)	0.3230(6)	0.2275(9)	1	0.8
Profile parameters						
pseudo-Voigt function						
$PV = \eta L + (1-\eta)G$		$\eta = 0.63(2)$				
Halfwidth parameters		$U = 0.015(3)$; $V = 0.015(3)$; $W = 0.0034(5)$				
Conventional Rietveld *R*-factors for points with Bragg contribution						
$R_{wp} = 27.8\%$; $R_{Bragg} = 7.8\%$; $S_{cor} = 2.99$						

Table 3
Structural parameters characteristics of the various Li_2MnO_3 samples deduced from the Rietveld refinement of their X-ray diffraction data according to the formula $\{(Li_2)_{2c}(Li_{4-y}Mn_y)_{4h}\}_{interslab}\{(Li_{2-z}Mn_z)_{2b}(Mn_{4-y-z}Li_{y+z})_{4g}\}_{slab}(O_{12})_{4i,8j}$.

Synthesis	Cell parameters				y	z	Percentage of Mn atoms in the interslabs (at.%)	Percentage of Mn atoms in Li sites in the slabs (at.%)
	a (Å)	b (Å)	c (Å)	β (°)				
Coprecipitation 650 °C for 24 h	4.9368(7)	8.517(1)	5.0195(8)	109.11(1)	0.320	0.712	5.3	35.6
Coprecipitation 850 °C for 24 h	4.9288(5)	8.5298(7)	5.0265(5)	109.216(7)	0.079	0.491	1.3	24.5
Solid state 800 °C for 4 h	4.9307(6)	8.531(1)	5.0242(6)	109.20(1)	0.097	0.589	1.6	29.5
Solid state 900 °C for 4 h	4.9292(2)	8.5315(3)	5.0251(5)	109.337(3)	0.056	0.292	0.9	14.6

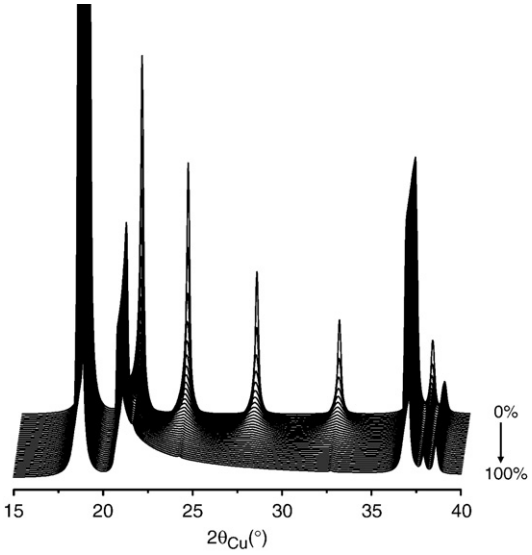

Fig. 4. Changes in the XRD patterns of Li_2MnO_3 as a function of the amount of stacking faults.

In Fig. 6b is given the comparison of the experimental XRD pattern with that calculated for a mixture of crystallites showing either the ideal stacking (80%) or the 100% faulted stacking (20%): this would correspond to the limit case with a maximum concentration of faults. Note that in that latter case, sharp (020), (110), (−111), (021) and (111) diffraction lines are expected, in addition to the asymmetric diffuse peak. As suggested by the experimental profile of the reflections (see insert of Figs. 3 and 6), the actual situation in the samples is probably between these two limit cases. Or in other words, the stacking faults are not statistically distributed in the material but are gathered in some parts of the crystals.

It is relevant that the amount of stacking faults evolves in accordance with the amount of exchange between lithium and manganese into the slabs; when the amount of faults decreases, the exchange decreases and reciprocally. This result shows that the Li/Mn exchange in the slabs quantified by the Rietveld refinement is in fact not related to a partial disorder in each slab between the two sites, but to a disorder occurring along the c monoclinic direction due to faults in the stacking of the ordered slabs. A localized stacking fault that leads to a shift in the *(a, b)* plane of a cationic ordered $(Li_{1/3}Mn_{2/3})$ plane induces changes in the occupancies of the manganese ions on the 2b site and of the lithium ions on the 4 g site because the structure is described, via the refinement, through an 'average' structural model in which all the cationic ordered $(Li_{1/3}Mn_{2/3})$ planes stack always according to the same stacking vector. Such stacking faults lead thus to an apparent statistical exchange between Mn and Li.

Note that these stacking faults are not expected to be at the origin of a Li/Mn exchange between the interslab and the slab. The peak shape presents some significant changes depending on the reflection as the amount of stacking faults increases, reflections (020) and (110) show for instance a huge broadening with an inversion of their intensities. The experimental profile can thus not be fitted correctly by a pseudo-Voigt profile function, inducing major discrepancies between the experimental and the calculated peak profiles that can be – from a calculation point of view – balance by changes in the sites occupancies and especially in the distribution of the electrons densities (or cations) between slabs and interslabs. According to this, presence of manganese ions in the interslab space – that remains low – is in our opinion just an artifact.

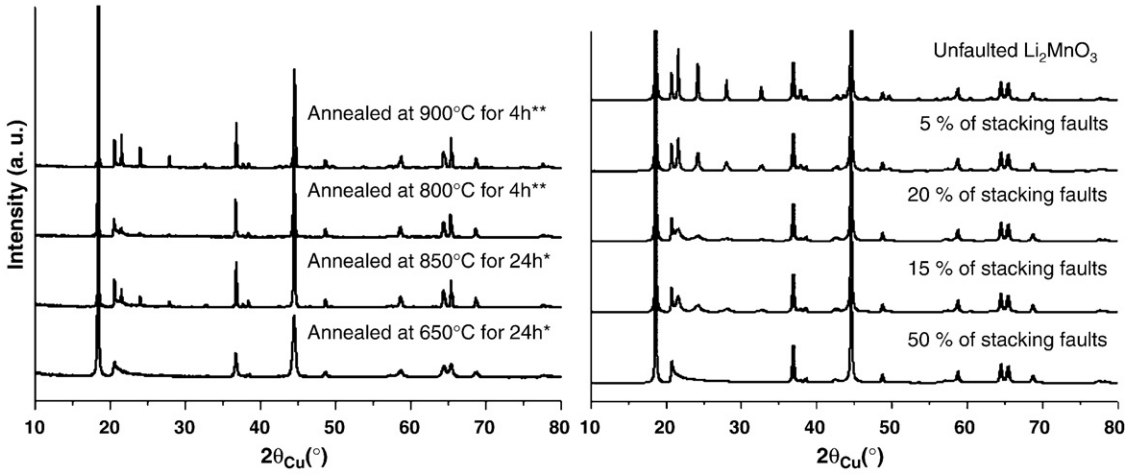

Fig. 5. Comparison of the XRD patterns collected for Li_2MnO_3 compounds obtained either by coprecipitation (*) or by solid state synthesis (**) with patterns calculated taking into account a given amount of stacking faults.

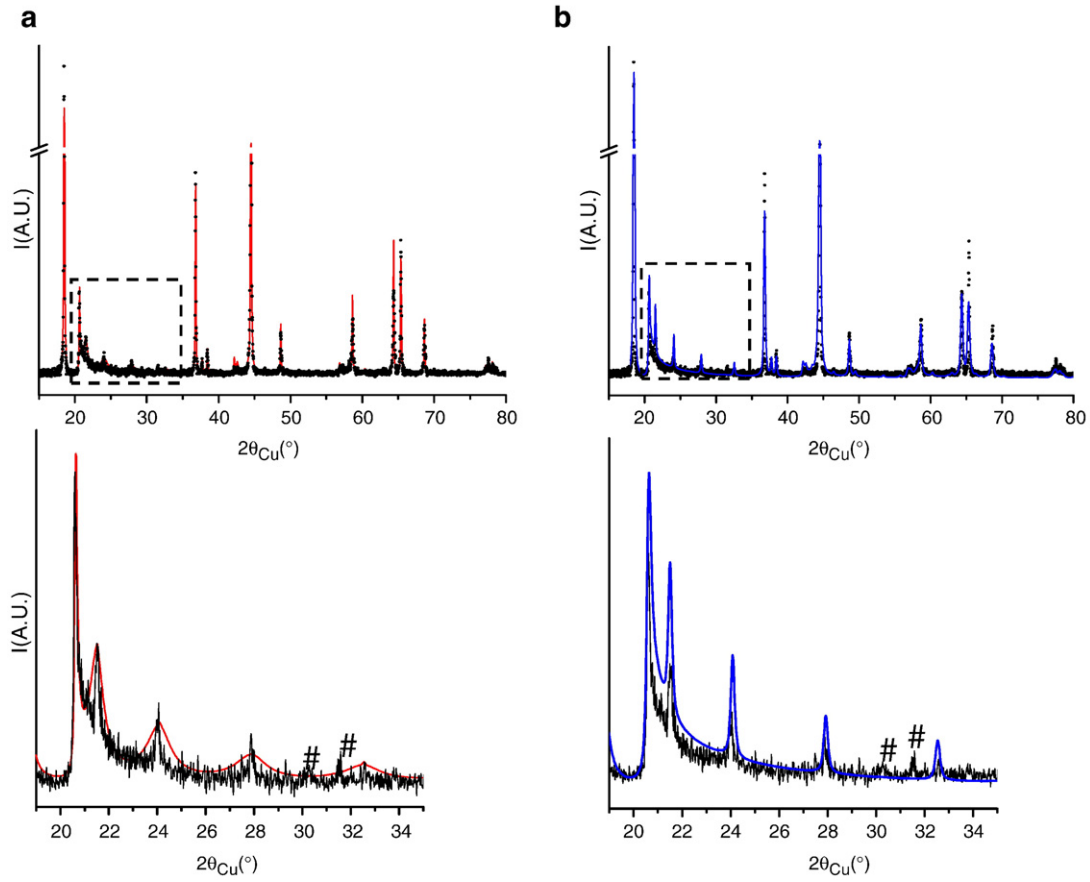

Fig. 6. Comparison of the XRD pattern collected for Li_2MnO_3 obtained by the solid state synthesis at 800 °C with: (a) that calculated considering 20% of statistically distributed stacking faults and (b) that calculated considering a mixture of crystallites, 20% being (largely) faulted and 80% showing ideal Li_2MnO_3 stacking. #: Li_2CO_3 impurity.

3.3. Electron diffraction study

Electron diffraction patterns collected along the [110] monoclinic zone axis are presented in Fig. 7 for our two extreme samples: the one synthesised by the coprecipitation route and annealed at 650 °C for 24 h and the second obtained by the solid state reaction and annealed at 900 °C for 4 h. Both patterns highlight the existence of diffuse scattering lines parallel to the c^* monoclinic axis. They are broad and no spots are distinguishable for the former material, whereas they are thinner and spots localized on the diffuse lines are clearly seen on the pattern related to the latter one. The location of the diffuse scattering lines confirms the existence of a superstructure and thus that lithium and manganese cations are ordered in the slabs whatever the synthesis route and the annealing treatment we performed. As stacking faults of the ordered cationic $(Li_{1/3}Mn_{2/3})$ planes occur along the c-axis, diffusion lines in the electron diffraction patterns can be their signatures. In the same way as for X-ray diffraction, we simulated the electron diffraction patterns along the [110] zone axis for various amounts of faults, see Fig. 8. It is relevant that spots affected by the diffusion become more and more extended to finish by composing an unbroken line when the disorder in the staking sequence along the c monoclinic axis is maximal. On the pattern

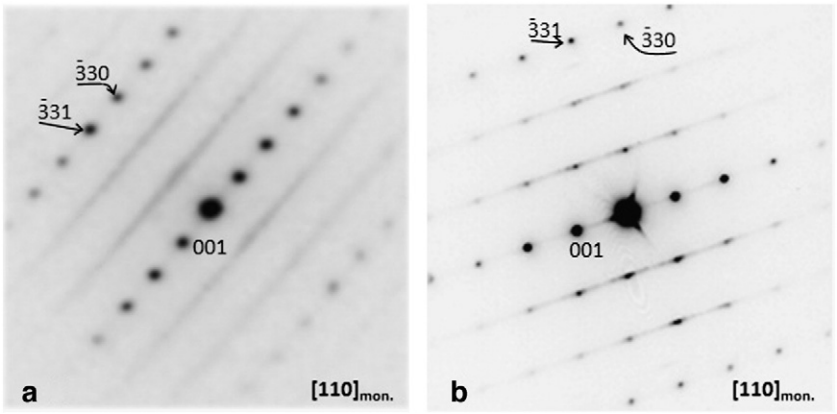

Fig. 7. Comparison of electron diffraction patterns obtained along the [110] monoclinic zone axis: a) for the coprecipitated sample annealed at 650 °C for 24 h and b) for the solid state synthesised one annealed at 900 °C for 4 h.

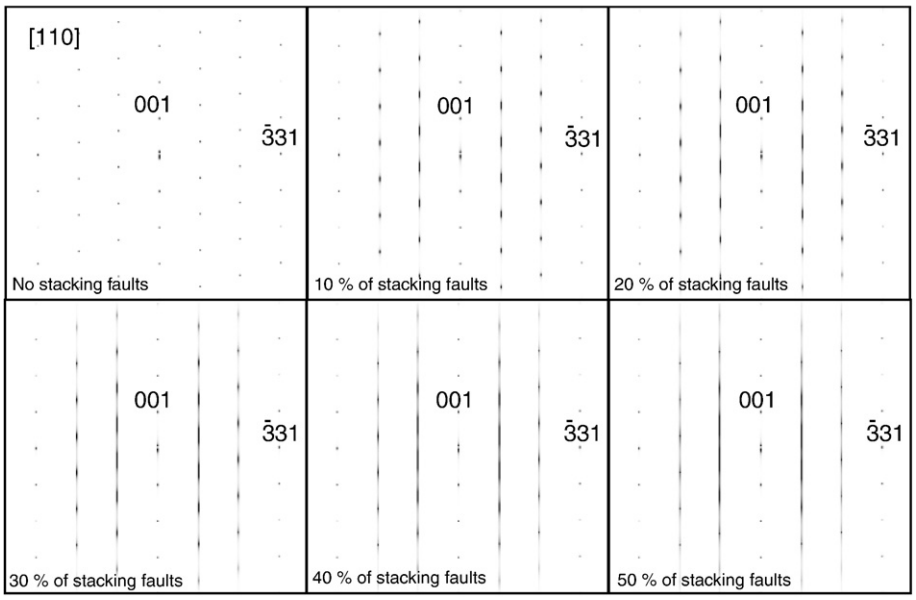

Fig. 8. Influence of stacking faults on the Li_2MnO_3 electron diffraction pattern obtained along the [110] monoclinic zone axis.

related to the sample synthesised by the solid state reaction, the localization of distinguishable spots on the diffuse scattering lines traduces the fact that ordered Li/Mn slabs are stacked preferentially according to the stacking vector (0; 0; 1) in monoclinic description, but the diffusion between the spots that still exist, traduces the existence of some disorder in this stacking.

On the basis of our description of the structural feature of Li_2MnO_3 (*i.e.* $(Li)_{interslab}(Li_{1/3}Mn_{2/3})_{slab}O_2$) the crystallographic properties of $Li_{1+x}(Ni_{0.425}Mn_{0.425}Co_{0.15})_{1-x}O_2$ with $x=0$ and $x=0.12$ that have been previously studied in our lab can be clarified. These materials adopt the α-$NaFeO_2$-type structure, described in the space group R-3m, with a cation distribution between the slab and the interslab space such as $(Li_{1-z}Ni^{II}_z)_{Interslab}(Li_{z+x}Ni_{0.425(1-x)-z}Mn_{0.425(1-x)}Co_{0.15(1-x)})_{Slab}$. As compared in Fig. 9 some of us already pointed out the existence of extra diffuse scattering lines parallel to the c^* direction in the reciprocal space of such materials. The position of these diffuse lines dividing by 3 the distance between two lines of spots perfectly indexed in the R-3m space group reveals a two dimensional superstructure ($\sqrt{3}.a_{hex}\times\sqrt{3}a_{hex}$) in the (a ; b) planes [10]. Contrary to Li_2MnO_3, the compositions of the studied materials do not allow a perfect cation distribution between the two crystallographic sites in the slabs [10,26]. Indeed, for $Li_{1.12}(Ni_{0.425}Mn_{0.425}Co_{0.15})_{0.88}O_2$ ($x=0.12$) it was shown that the slab composition was $Li^+_{0.14}Ni^{2+}_{0.114}Ni^{3+}_{0.24}Mn^{4+}_{0.374}Co^{3+}_{0.132}$ [9,27] with the "big cations" (Li^+, Ni^{2+}) occupying the larger cation site in the slab and the "small cations" (Ni^{3+}, Mn^{4+}, Co^{3+}) occupying mainly the smaller one. In fact the (Li^+, Ni^{2+})/(Ni^{3+}, Mn^{4+}, Co^{3+}) ratio is 0.74 whereas the "big cations"/"small cations" ratio implying the perfect order is 0.5. For $LiNi_{0.425}Mn_{0.425}Co_{0.15}O_2$ ($x=0$) this ratio becomes 0.37. For $x=0$, the presence of unbroken diffuse scattering lines indicates the lack of correlation between the transition cations planes whereas, for $x=0.12$ the diffuse scattering lines are still observed but the intensity along these lines is not uniform anymore: a higher intensity is observed at the positions where the *C*2/*m* reflexions of Li_2MnO_3 are located which means that the stacking of the ordered plane tends to be that observed in this former compound. This trend can be related to the evolution of the cation distribution in the materials. Indeed, the difference between the $x=0$ and the $x=0.12$ material is the ratio "big cations"/"small cations" which is more or less close to 0.5 (0.74 *vs.* 0.37) implying a less long

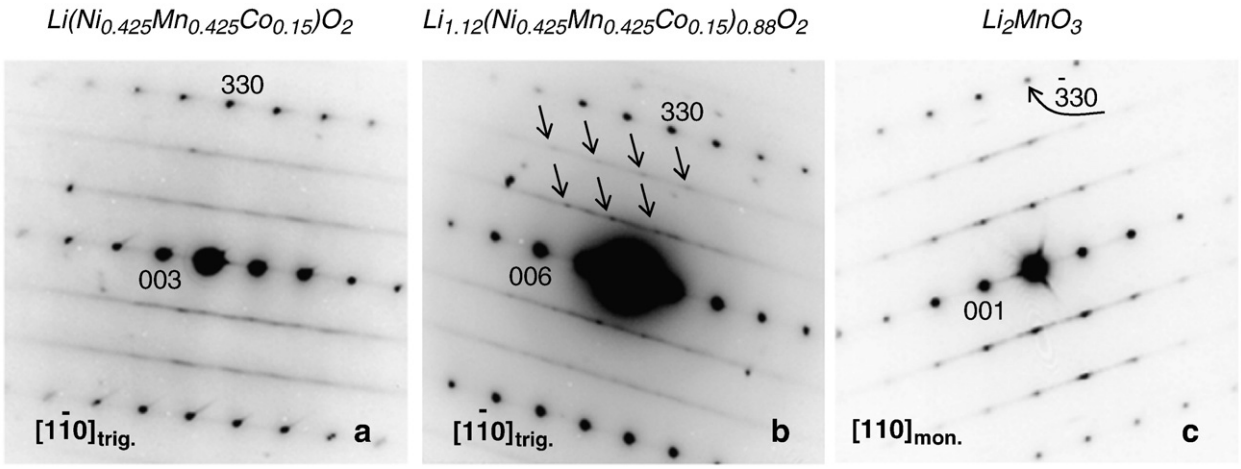

Fig. 9. Comparison of the $[1\text{–}10]_{trig.}$ zone axis patterns of the materials $Li(Ni_{0.425}Mn_{0.425}Co_{0.15})O_2$ and $Li_{1.12}(Ni_{0.425}Mn_{0.425}Co_{0.15})_{0.88}O_2$ respectively in a) and b) with the $[110]_{mon.}$ zone axis pattern of Li_2MnO_3 synthesised at 900 °C for 4 h by the solid state synthesis in c). In b) the arrows underline the reflections appearing in the diffuse lines and located as in c).

range in plane cation ordering and as a consequence a smaller driving force to order the slabs along the *c*-axis.

4. Conclusion

We have studied various Li_2MnO_3 samples obtained via two synthesis routes and different annealing treatments. X-ray and electron diffraction revealed that it was not possible to synthesize the ideal compound, *i.e.* free of stacking faults, via these syntheses. Indeed, we demonstrate that the ordered ($Li_{1/3}Mn_{2/3}$) cationic planes are never perfectly stacked along the *c*-axis as it should be when the structure of this compound is described using the C2/*m* space group. The frequency of the stacking faults depends on the temperature of the thermal treatment used during the synthesis: the higher the temperature is the lower the frequency. A similar evolution, in function of the stoichiometry, has been pointed out for the $Li_{1+x}(Ni_{0.425}Mn_{0.425}Co_{0.15})_{1-x}O_2$ compounds. Depending of the composition, and then of the more or less adequacy of the stoichiometry to the order in the cationic layer, the stacking along *c* of the ordered cationic planes presents a variable number of defects.

Acknowledgments

The authors want to thank Philippe Dagault, Jérémy Humez and Laëtitia Etienne from ICMCB for their technical assistance, as well as the Région Aquitaine and the Ministère de l'Enseignement Supérieur et de la Recherche for financial support.

References

[1] K. Mizushima, P.C. Jones, P.J. Wiseman, J.B. Goddenough, Mater. Res. Bull. 15 (1980) 783.
[2] A. Broussely, P. Blanchard, P. Biensan, J.P. Planchat, K. Nechev, R.J. Staniewicz, J. Power Sources 119 (2003) 859.
[3] M. Guilmard, L. Croguennec, D. Denux, C. Delmas, Chem. Mater. 15 (2003) 4476.
[4] T. Ohzuku, Y. Makimura, Chem. Lett. (2001) 744.
[5] T. Ohzuku, Y. Makimura, Chem. Lett. (2001) 642.
[6] S.W. Oh, S.H. Park, C.W. Park, Y.K. Sun, Solid State Ion. 171 (2004) 167.
[7] S. Jouanneau, J.R. Dahn, J. Electrochem. Soc. 151 (2004) A1749.
[8] S. Jouanneau, D.D. MacNeil, Z. Lu, S.D. Beattie, G. Murphy, J.R. Dahn, J. Electrochem. Soc. 150 (2003) A1299.
[9] N. Tran, L. Croguennec, C. Labrugère, C. Jordy, Ph. Biensan, C. Delmas, J. Electrochem. Soc. 153 (2) (2006) A261.
[10] F. Weill, N. Tran, L. Croguennec, C. Delmas, J. Power Sources 172 (2007) 897.
[11] P. Strobel, B. Lambert-Andron, J. Solid State Chem. 75 (1988) 90.
[12] R.D. Shannon, C.T. Prewitt, Acta Crystallogr., B 25 (1969) 925.
[13] G. Lang, Z. Anorg. Allg. Chem. 348 (1966) 246.
[14] J. Bréger, M. Jiang, N. Dupré, Y.S. Meng, Y. Shao-Horn, G. Ceder, C.P. Grey, J. Solid State Chem. 178 (2005) 2575.
[15] V. Jansen, R. Hoppe, Z. Anorg. Allg. Chem. 397 (1973) 297.
[16] A. Riou, A. Lecerf, Y. Gerault, Y. Cudennec, Mater. Res. Bull. 27 (1992) 269.
[17] V. Massarotti, M. Bini, D. Capsoni, A. Altomare, A.G.G. Moliterni, J. Appl. Crystallogr. 30 (1997) 123.
[18] Y.S. Meng, G. Ceder, C.P. Grey, W.-S. Yoon, M. Jiang, J. Bréger, Y. Shao Horn, Chem. Mater. 17 (2005) 2386.
[19] Y.S. Meng, G. Ceder, C.P. Grey, W.-S. Yoon, Y. Shao Horn, Electrochem. Solid-state Lett. 7 (6) (2004) A155.
[20] A. Boulineau, L. Croguennec, C. Delmas and F. Weill, to be submitted to Chem. Mater.
[21] W. Zhang, Y. Liu, Z. Yang, S. Tang, M. Chen, Solid State Commun. 131 (2004) 441.
[22] J. Rodríguez-Carvajal, *Laboratoire Léon Brillouin, http://www-llb.cea.fr/fullweb/powder.htm*.
[23] M.M.J. Treacy, J.M. Newsam, M.W. Deen, Proc.Roy. Soc. Lond. A433 (1991) 499.
[24] A. Boulineau, L. Croguennec, C. Delmas and F. Weill, *Chem. Mater.* doi:10.1021/cm900998n.
[25] A. Rougier, P. Gravereau, C. Delmas, J. Electrochem. Soc. 143 (1996) 1168.
[26] F. Weill, N. Tran, N. Martin, L. Croguennec, C. Delmas, Electrochem. Solid-state Lett. 10 (8) (2007) A194.
[27] N. Tran, L. Croguennec, C. Labrugère, C. Jordy, Ph. Biensan, C. Delmas, Electrochem. Soc. 153 (2) (2006) A261.